An Alternative Method for Characterization and Comparison of Plant Root Shapes

A thesis submitted to the
College of Graduate and Postdoctoral Studies
in partial pulfillment of the requirements
for the degree of Master of Science
in the Department of School of Environment and Sustainability
University of Saskatchewan
Saskatoon

By
Yujie Pei

Contents

Existing Morphological Descriptors for Root Systems

1.1 Background

1.1.1 Importance of Roots

- Mechanical and functional abilities of plant roots

- Plant root plasticity in the resource-limited environment

1.1.2 Importance of Research

1.1.2.1 Demand in crop breeding programs

1.1.2.2 Environment and Sustainability

- reduce the negative impacts of fertilization
- high crop productivity to feed the increasing global population

1.1.3 Promising application in other branching structures

- Trees
- River networks in geography
- Blood vessels in medicine
- Leaf vein networks

1.2 Summary of Existed Descriptors

1.2.1 Metric

1.2.1.1 Basic Geometric Descriptors

- maximum depth
- maximum width
- etc.

1.2.1.2 Compound Descriptors (Computed From the Basic Descriptors)

- Density
- aspect ratio
- etc.

1.2.1.3 Weaknesses

- Rely on the resolution of the images [3]
- Only provide a general view of root morphology [3]
- Difficult to assess the spatial configuration of roots
- Fail to describe the full complexity of root systems

1.2.2 Non-metric

1.2.2.1 Topological Analysis

- Persistent homology [28]
  - Persistence barcode shows the number of branches.
  - Persistence barcode indicates how branched roots connect along the scale of the function (e.g. geodesic distance).
  - Compare the similarity of branching structures by a pair-wise distance matrix using the bottleneck distance method.
- Horton-Strahler index [32]
  - Categorize the topological complexity of the whole branching structure.
  - Provide a numerical measure of connectedness and complexity of the branching at each vertex by a dimensionless ratio: bifurcation ratio.
  - The range of index and the length ratio indicate the size of the branching structure.
- Fractal Analysis [31]
  - Measure the complexity of branching structures.
  - Measure self-similarity of branching structures by fractal dimension of the root systems.

1.2.2.2 Strengths

- Highly complementary to geometric descriptors to characterize how individual roots are connected through branching [6].
- Describe branching structures independent of transformation and deformation.

1.2.2.3 Problems and Weaknesses

- Only analyze the connectedness of branching structures, which is a portion of the complexity of plant root systems.
- Fail to characterize spatial distribution.
- Some biologically topological indices analyze the root growth qualitatively based on line-linked systems [11], but not characterize the mathematical topological properties.
- The fractal analysis aims to describe self-similar structures, which grow by continually repeating simple growth rules [12].

1.3 Problem Statements

...

An Alternative Mathematical Method for Shape Description

2.1 Kac's Idea: Can One Hear the Shape of a Drum? [22]

2.1.1 Interpretations of Kac's Problem

- When the drum vibrates, one can hear the sound, which is composed of tones of various frequencies. How much can shape features be inferred from hearing a discrete spectrum of pure tones produced by a drum?

- If a complete sequence of eigenvalues of the Dirichlet problem for the Laplacian can be obtained precisely, will people determine the shape of a planar?

2.1.2 Problem Statement

- Consider a simply connected membrane Ω in the Euclidean space bounded by a smooth convex curve $\partial\Omega$ (e.g. a drum without any holes)
- Find function ϕ on the closure of Ω, which vanishes at the boundary $\partial\Omega$, and a number λ satisfying $-\Delta\phi = \lambda\phi$.
  - Δ is the Laplace operator. e.g. $\Delta = \sum_{i=1}^{n} \frac{\partial^2}{\partial x_i^2}$ in Cartesian coordinate system.
  - If there exists a solution $\phi \neq 0$, the corresponding λ is defined as a Dirichlet eigenvalue.
  - For each domain Ω, there has a sequence of eigenvalues $\lambda_1, \lambda_2, \lambda_3, ...$ corresponding to a set of eigenfunction $\phi_1, \phi_2, \phi_3, ...$
  - ϕ_k form an orthonormal basis of $L^2(\Omega)$ of real valued eigenfunctions; the corresponding discrete Dirichlet eigenvalues are positive ($\lambda_k \in \mathbb{R}^+$).
- An important function [16]:

$$h(t) = \sum_{k=1}^{\infty} e^{-\lambda_k t} \tag{2.1}$$

  - It is a Dirichlet series.
  - It is called the spectral function or the heat trace.
  - It is smooth and converges for every $t > 0$.

2.1.3 Summarize the Results of Kac's Idea

$$h(t) = \sum_{k=1}^{\infty} e^{-\lambda_k t} \sim \frac{|\Omega|}{2\pi t} - \frac{L}{4}\frac{1}{\sqrt{2\pi t}} + \frac{1}{6} \tag{2.2}$$

- As $t \to 0^+$, the leading terms of the asymptotic expansion of $h(t)$ imply the geometrical attributes of Ω
  - the total area
  - the perimeter
  - the curvature
- If the domain Ω has the polygonal boundary, the third term shows in the information about the interior angles of the polygon [16].

2.1.4 Conclusion

2.1.4.1 Advantages

- Kac proposed a novel analytical mathematical method for the shape description without using measuring tools, e.g. rulers.
- Other mathematicians extended Kac's idea in exploring the geometrical information of more complex domains with various boundary conditions [26][14][13] [35][30].

2.1.4.2 Limitations

- It is only available for the convex domain, which has a smooth or piecewise smooth boundary.
- Except in very few cases (i.e. rectangular, disk, certain triangles), the complete sequence of eigenvalues λ_k can not be calculated [16].
- Only the first few terms in the asymptotic expansion of $h(t)$ are explicitly available.

2.2 Extended Work of Kac's Idea [7][33]: Heat Content

2.2.1 Fouier's Heat Equation [4]

- Mathematical Formula

$$\frac{\partial u(\boldsymbol{s},t)}{\partial t} = \Delta u(\boldsymbol{s},t) \tag{2.3}$$

- Interpretation

  It is a deterministic model used to characterize the evolution of quantities over the space and time. (e.g. the flow of heat)

2.2.2 Summarize the Idea

- Initial-Boundary Value Problem (IBVP)

  $u(\boldsymbol{s}, t)$ indicates the value of the tempretature at $\boldsymbol{s} \in \Omega$ at time t satisfying Eq. 2.3 and

  - Initial condition: $u(\boldsymbol{s}, t) = f(\boldsymbol{s})$ as $t \to 0$.
  - Dirichlet boundary condition: $u(\boldsymbol{s}, t) = 0$ for $\boldsymbol{s} \in \partial\Omega$

    It is also called the absorbing boundary condition; i.e. any molecule will be instantly absorbed when it touches the boundary $\partial\Omega$;

- A Basic Integration

$$\beta_\Omega(f, g)(t) = \int_\Omega \int_\Omega H_\Omega(\boldsymbol{s}, t|\boldsymbol{s_0}) f(\boldsymbol{s_0}) g(\boldsymbol{s}) d\boldsymbol{s_0} d\boldsymbol{s} \tag{2.4}$$

$$= \int_\Omega u(\boldsymbol{s}, t) g(\boldsymbol{s}) d\boldsymbol{s} \tag{2.5}$$

  - $H_\Omega(\boldsymbol{s}, t|\boldsymbol{s_0})$ is called the heat kernel of Ω describing the density of the heat at $\boldsymbol{s}$ after time t when initially there is only one single hot source at $\boldsymbol{s_0}$.
  - $u(\boldsymbol{s}, t)$ is the general solution to Eq. 2.3, which can be expressed as the convolution of the initial condition with the heat kernel of the domain.
  - $g(\boldsymbol{s})$ is an auxiliary test function for studying the distributional nature of the tempretature function $u(\boldsymbol{s}, t)$ near $\partial\Omega$.

- Heat Content Calculation

  Given

$$g(\boldsymbol{s}) = 1 \tag{2.6}$$

$$Q_\Omega(t) = \int_\Omega \int_\Omega H_\Omega(\boldsymbol{s}, t|\boldsymbol{s_0}) f(\boldsymbol{s_0}) d\boldsymbol{s_0} d\boldsymbol{s} \tag{2.7}$$

$$= \int_\Omega u(\boldsymbol{s}, t) d\boldsymbol{s} \tag{2.8}$$

- Shape Characterization

  - As $t \to 0^+$, $Q_\Omega(t) \simeq \sum_{n=1}^{\infty} \beta_n(\Omega) t^{\frac{n}{2}}$
  - Obtain geometrical information of Ω from β_n
    - area
    - length
    - scalar curvature
    - mass

2.2.3 Conclusion

- Strengthness
  - Instead of calculating a complete sequence of the Dirichlet eigenvalues for exploring the shape attributes of geometry, the asymptotic expansion of the heat content, defined as integrating the solution to the heat equation over the space-dimension, also implies the geometrical characteristics.
- - Only the infinitly differentiable boundary $\partial\Omega$ is considered.
  - Only the first few terms in the asymptotic expansion are explicitly known.
  - Either irregular geometries or discontinuities lead to the complexities, so the explicit solutions $u(\boldsymbol{s}, t)$ are close to non-existed.
  - The numerical evaluation of the analytical $u(\boldsymbol{s}, t)$ and $Q_\Omega(t)$ is usually by no means trivial because they are in the form of infinite series.
  - Similiarly, only the first few coeffients β_n in the asymptotic expansion of $Q_\Omega(t)$ can be expressed as the complicated explicit forms.

2.3 Monte Carlo Simulation for Approximating Heat Content $Q_\Omega(t)$

2.3.1 Background [21]

2.3.1.1 Stachasic Differential Equations (SDEs)

- Stochastic process
- Brownian motion

2.3.1.2 Connection Between SDEs and Heat Equation

- Ito calculus
- Intepretating the heat equation by the probability density of particles undergoing Brownian motion

2.3.2 A Special Case of Heat Content Calculation

- Uniform initial tempretaure distribution in Eq. 2.7

$$f(\boldsymbol{s_0}) = \frac{1}{|\Omega|} \tag{2.9}$$

  - $|\Omega|$ is the area of the domain Ω.
  - Particles's initial positions are distributed uniformly in Ω.

- Intepretation of Eq. 2.6: observing all the Brownian particles unbiasedly.

- Probabilistic Intepretation of Heat Kernel $H_{\Omega}(\boldsymbol{s}, t|\boldsymbol{s_0})$: conditional probability density function of Brownian particles

- Probabilistic Interpretation of $Q_{\Omega}(t)$: Survival Probability $S_{\Omega}(\tau)$

  - First passgae time τ: the time taken by the particle to encounter the absorbing boudary $\partial\Omega$ from the initial position.
  - Derivation of $S_{\Omega}(\tau)$ based on $H_{\Omega}(\boldsymbol{s}, t|\boldsymbol{s_0})$.

2.3.3 Monte Carlo Simulation (LRWs) for approximating $S_\Omega(\tau)$

2.3.3.1 Monte Carlo Integration

- Introduction
  - Definition: utilizing the random sampling of a function to compute an estimate of its integral numerically [18].
  - Uniform Sampling Method
- Given an initial position $\boldsymbol{s_0} \in \Omega$, approximating $H_\Omega(\boldsymbol{s}, t|\boldsymbol{s_0})$ by simulating the trajectories of a large number of particles by Lattice Random Walks (LRWs).
- Sampling a lager number of particles, whose initial sites are distributed uniformly within Ω to estimate $S_\Omega(\tau)$.

2.3.3.2 Design LRWs in the $2-$ dimensional image

- Initial condition: uniform distribution within Ω, which is bounded by the border of the image and the edge of the target object.
- Boundary condition
  - Perodic boundary condition the edges of the image;
  - Absorbing boundary condition on the boundary of the target shape.

2.3.3.3 Sample Size Determination - Dvoretzky–Kiefer–Wolfowitz (DKW) inequality [9]

- Mathematical formula and interpretation
- Strengths
  - Distribution-free
  - Sample size calculation does not depend on
    - Domain shape and size
    - Target geometry
    - B.C.s

2.3.3.4 Output Analysis (in theory)

- Kaplan-Meier Estimator [24] [1]
- Confidence Interval [15] [20] [23][29]
- Two-Sample Statistical Tests (weighted logrank tests) [5] [2] [25] [27] [10] [19]
  - Wilcoxon
  - Tarone-Ware
  - Peto
  - Fleming-Harrington

LRWs in Artificial Images

The fixed-time step Monte Carlo simulation, LRWs, has been validated in the annulus in Appendix B by comparing the analytical and numerical survival function. The further validation of LRWs is to distinguish the geometries and explore their structural features from both short and long time survival behaviours.

3.1 Circle and Rectangle Yuge

Given two simple convex shapes with the same area, circle and rectangle, we are interested in how and whether their corresponding survival curves differ from each other. For the equal-area geometries, rectangle and circle, Eq. 2.2 indicates that the survival function of the former decays faster than the latter as the time approaches zero.

The preliminary step of testing the research hypothesis is to generate two black-and-white images with the same dimensions as shown in Fig. C.1. In the binary images, circle and rectangle have an equal number of white pixels. For simplicity, the centroid of shapes located at the center of the image. Then, simulating LRWs in the images and estimating survival functions by Kaplan-Meier estimator.

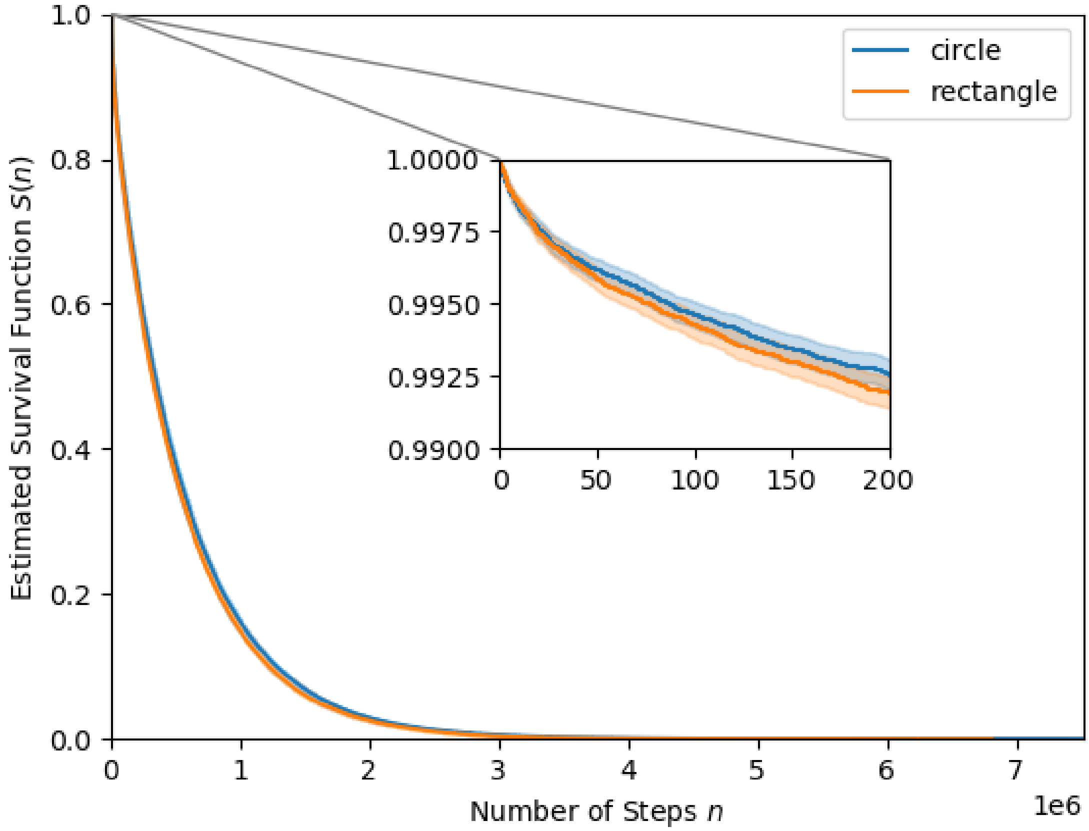

Figure 3.1: In the inset, the decay rate of the survival function for the rectangle is slightly larger than for the circle, which coincides with the theoretical result.

3.1.1 Output Analysis

The differences between survival functions for the circle and rectangle are not visible. Moreover, the approximate 95% confidence intervals of the survival functions overlap. In this case, non-parametric statistical tests can be used to compare entire survival distributions and assess their dissimilarities. The logrank test has maximum power if the proportional hazards assumption is satisfied.

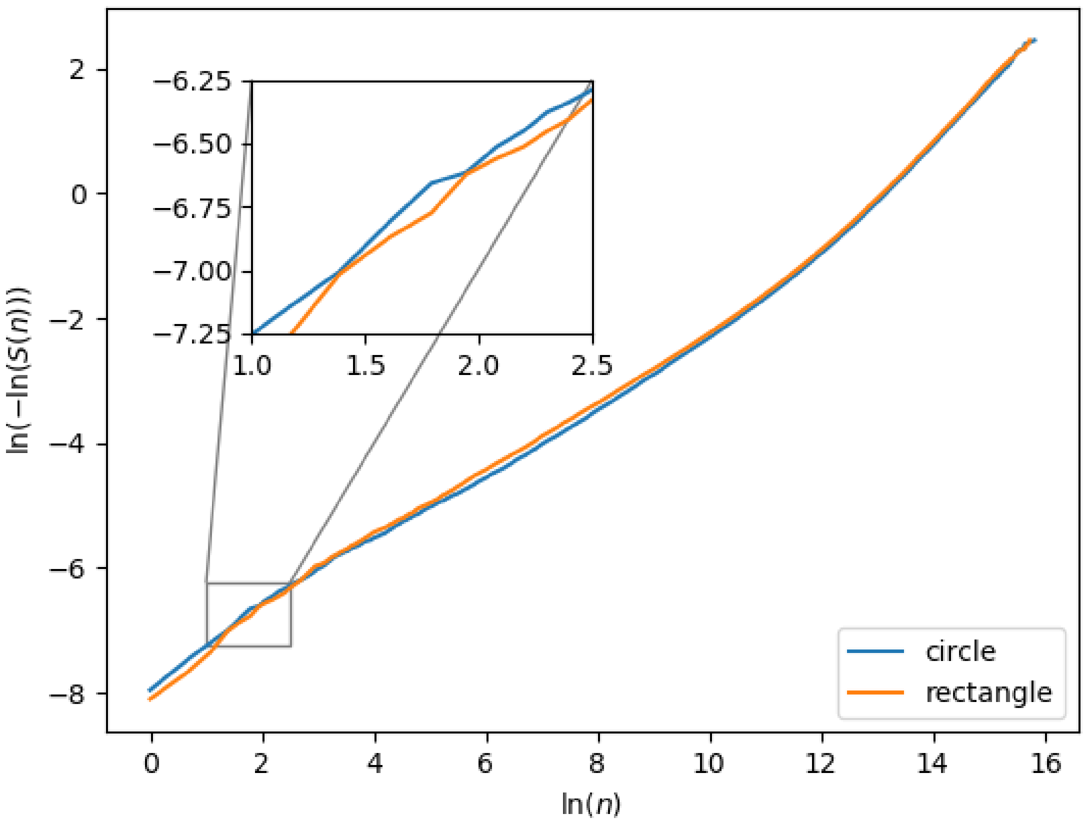

Figure 3.2: It is a graphical method for checking proportionality by looking for parallelism. As shown in the inset plot, two curves cross at some points and their shapes vary over time. Moreover, $p < 0.05$ in the non-proportional test. Thus, the survival functions for circle and rectangle do not satisfy the proportional hazard assumption.

	test_statistic	p
Logrank	137.23	0.0
Tarone-Ware	134.31	0.0
Gehan-Breslow	123.83	0.0
Fleming-Harrington	123.83	0.0

Table 3.1: Survival functions for circle and rectangle are statistically different since p values equal zeros.

3.1.2 Conclusion

Although the proportional hazard assumption test is failed as shown in Fig. **??**, the weighted logrank tests indicate that the null hypothesis should be rejected. In conclusion, LRWs is an alternative tool to quantify and distinguish the geometries in the $2-$ dimensional image without measuring the predefined shape descriptors.

3.2 Complicated Branching Structures

In the preceding section, the research hypothesis has been tested by the comparison of simple shapes. More complex branching structures, as shown in Fig. C.2 and Fig. C.3, are produced in this section for further validation of the research assumption and understanding of the survival curve. The branching structures in the images are equal-area and vertically symmetric, but the template in G_1 is shorter and narrower than in G_2. In G_i, $i = 1, 2$, the larger number of iterations j, the more complicated structures L_j, $j = 3, 4, 5, 6$, with more nodes.

		p			
		Logrank	TW	GB	FH
G_1 L_3	G_1 L_4	0.0	0.0	0.0	0.0
	G_1 L_5	0.0	0.0	0.0	0.0
	G_1 L_6	0.0	0.0	0.0	0.0
G_1 L_4	G_1 L_5	0.1773	0.0	0.0	0.0
	G_1 L_6	0.0	0.0	0.0	0.0
G_1 L_5	G_1 L_6	0.0	0.0	0.0	0.0

Table 3.2

		p			
		Logrank	TW	GB	FH
G_2 L_3	G_2 L_4	0.0	0.0	0.0	0.0
	G_2 L_5	0.0	0.0	0.0	0.0
	G_2 L_6	0.0	0.0	0.0	0.0
G_2 L_4	G_2 L_5	0.0	0.0	0.0	0.0
	G_2 L_6	0.0	0.0	0.0	0.0
G_2 L_5	G_2 L_6	0.0	0.0	0.0253	0.0253

Table 3.3

3.2.1 Output Analysis of $S(R)$

3.2.1.1 Interpretation of Survival Curves

3.2.1.2 Comparison of Survival Curves

3.2.1.3 Distance Matrices

3.2.1.4 Multidimenisonal Scaling

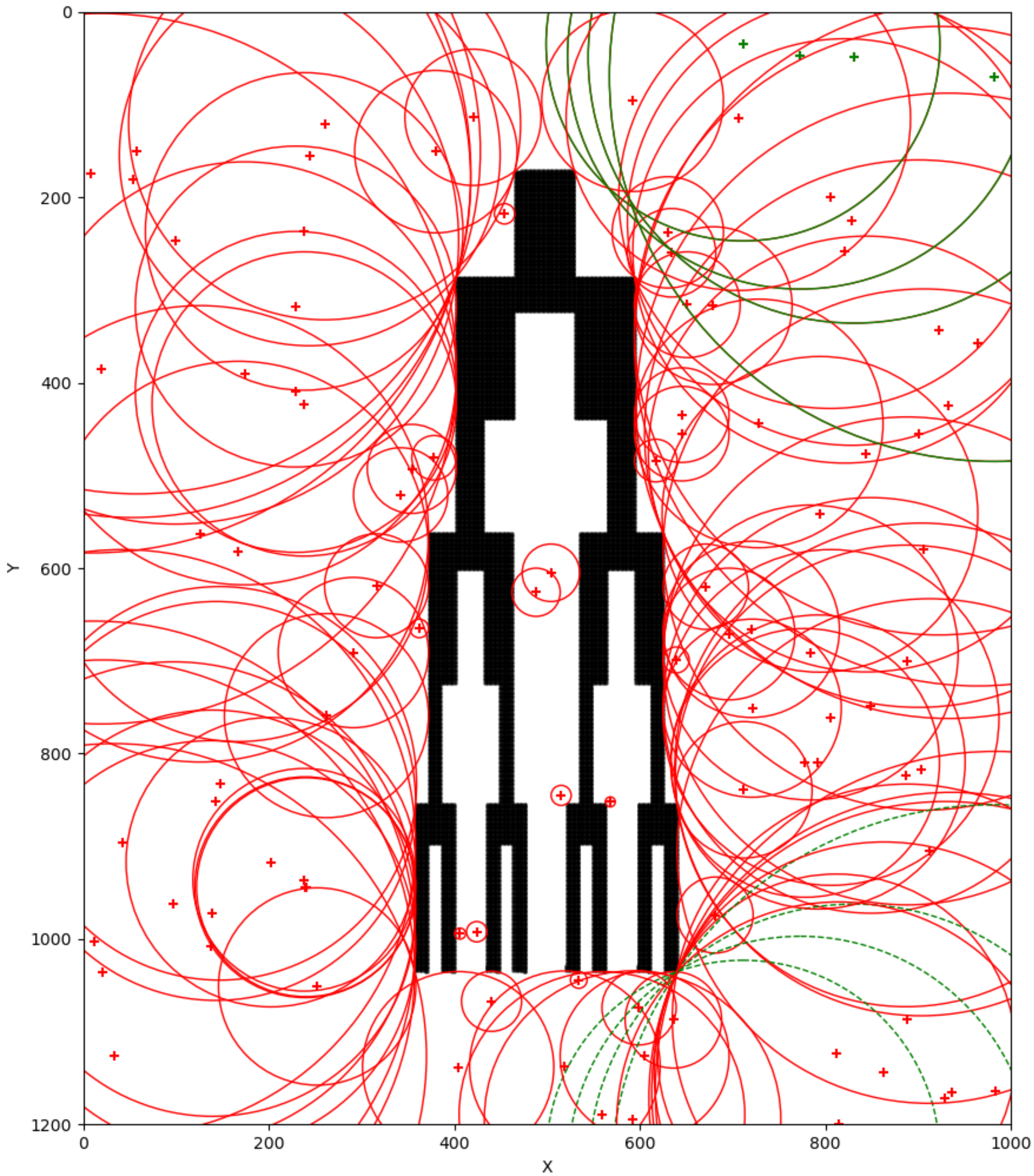

Figure 3.3: first circles

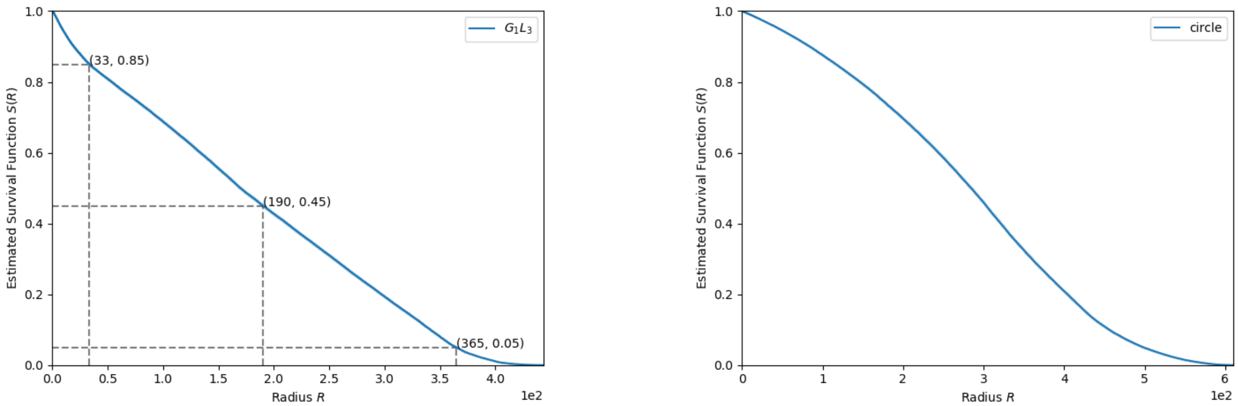

(a) **(b)**

Figure 3.4

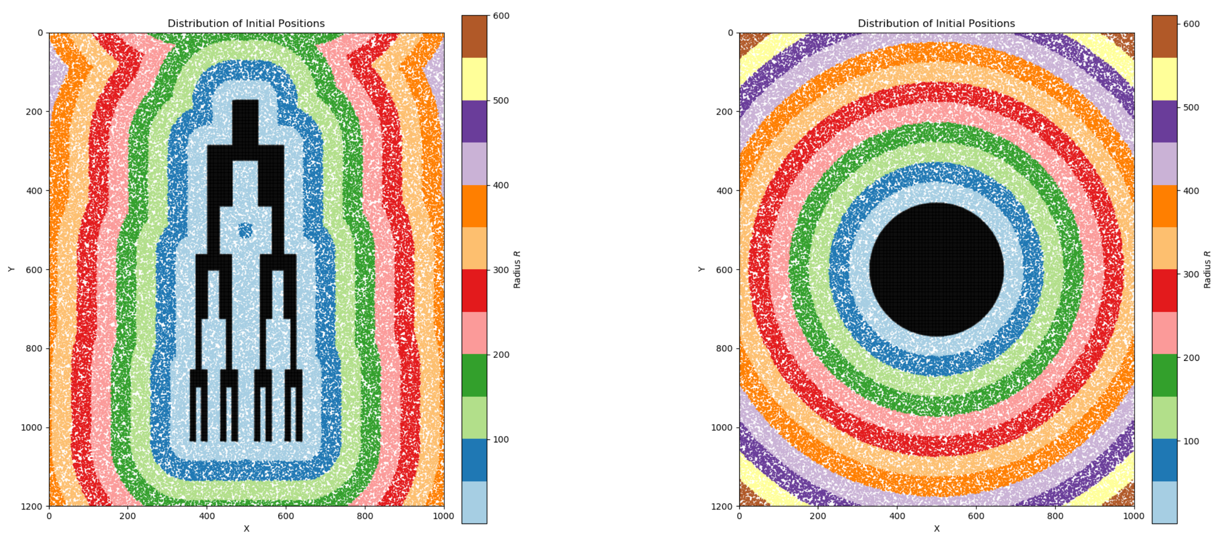

(a) **(b)**

Figure 3.5

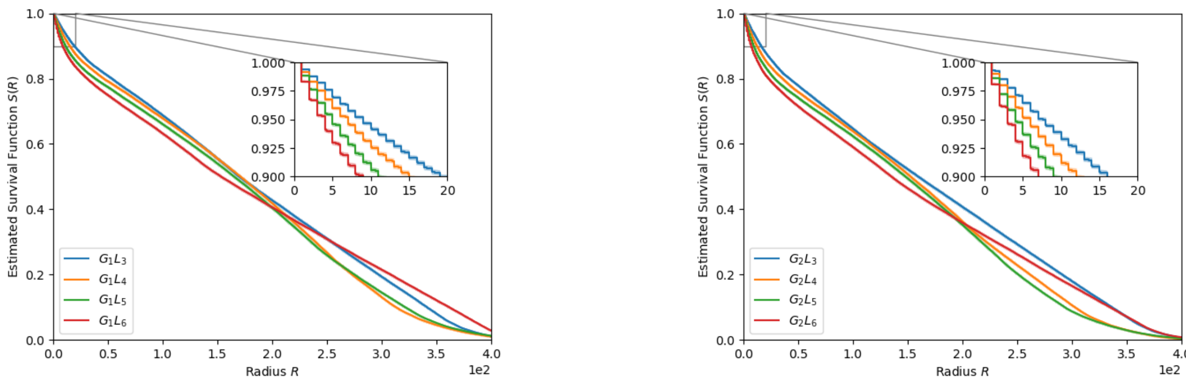

(a) **(b)**

Figure 3.6

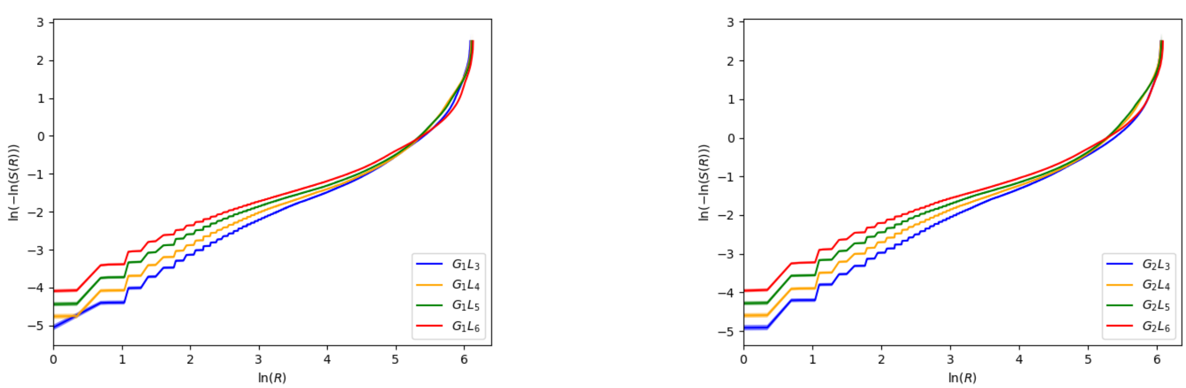

(a) **(b)**

Figure 3.7

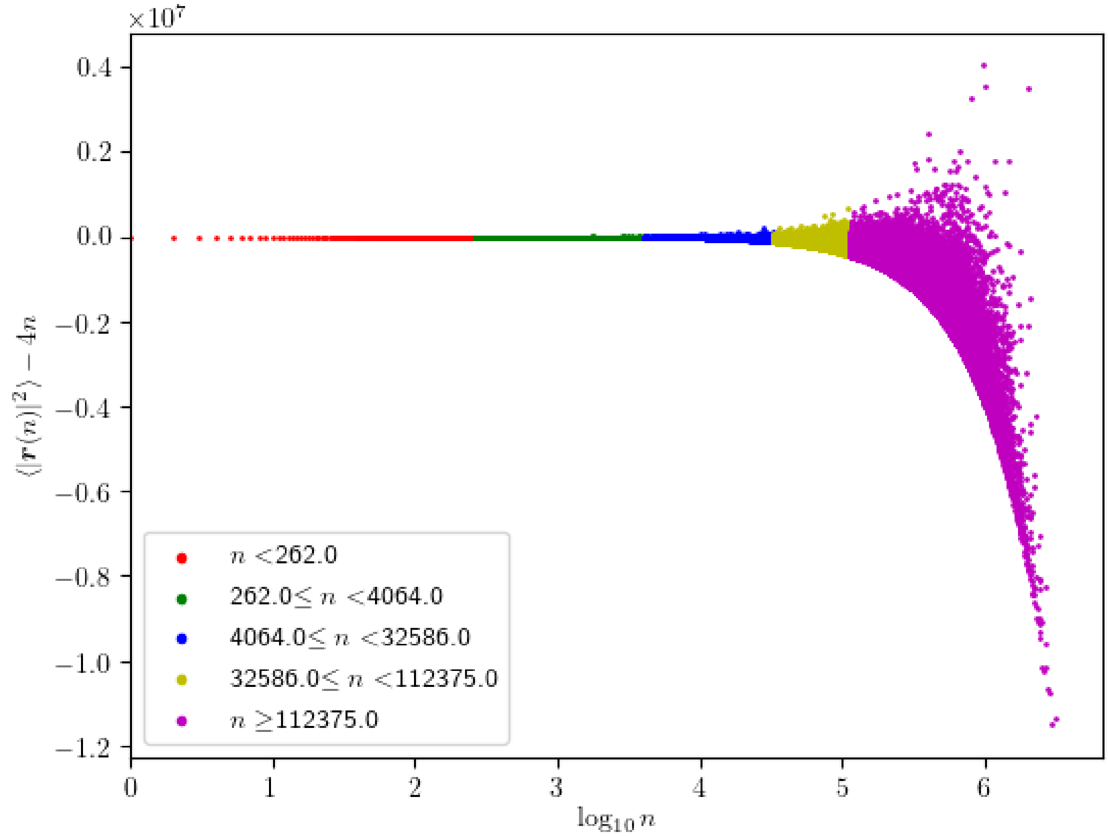

Figure 3.8: Particles in G_1L_3 are divided into several subgroups based on various intervals of steps, and their colours are as identical as the segments in Fig. 3.10a.

3.3 Output Analysis of $S(n)$ and $S(d)$

3.3.1 Relationship Between n and d

In this section, the displacement of a particle, d, is the shortest distance from the initial to the stop position in the infinite tiling plane. In theory, the mean square displacement (MSD) of N Brownian particles at $n-$th step in 2−dimensional space is defined as

$$MSD = \langle |\boldsymbol{r}(n)|^2 \rangle = \frac{1}{N}\sum_{i=1}^{N}(\boldsymbol{s}_i(n) - \boldsymbol{s}_i(0))^2 = 4Dn \tag{3.1}$$

where the subscript, i, refers to each particle for which the MSD is calculated. $\boldsymbol{s}_i(n)$ and $\boldsymbol{s}_i(0)$ are the $i-$th particle positions at $n-$th step and at the initial time, respectively. D is diffusion coefficient which is related to the variance of the independent displacements of the particle. In the simulation, D equals 1.

Eq. 3.1 indicates a linear relationship between the mean square displacement of the particle and the

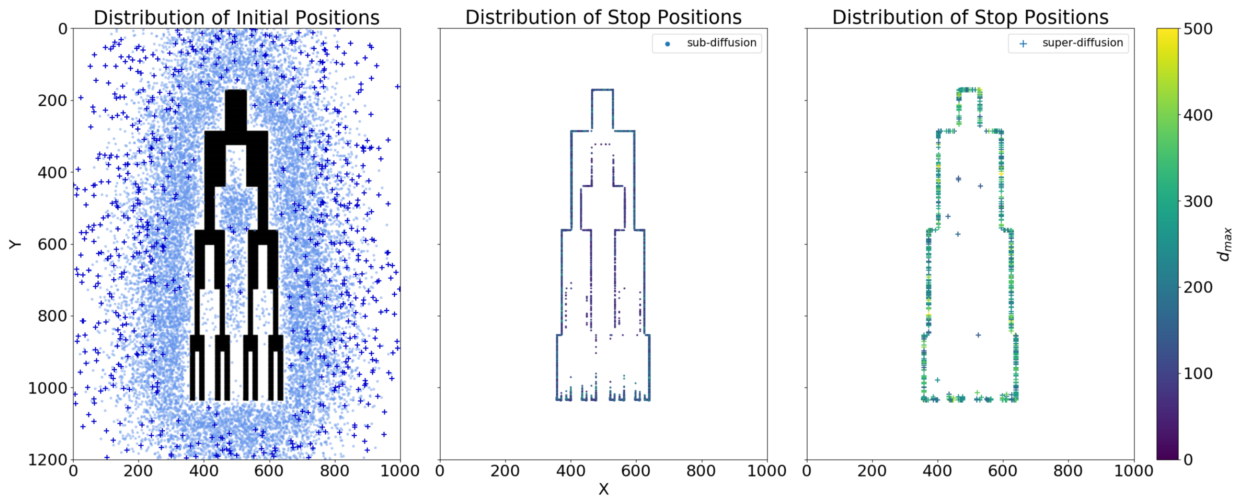

Figure 3.9: In the left figure, 696 dark blue pluses refer to super-diffusion particles, which are distributed closer and more concentrated to the fringe of the branching structure. 15198 pale blue points represent sub-diffusion particles and scatter mainly around the edges of the image. In-between the branches, there has only six super-diffusion particles and an enormous amount of sub-diffusion ones. The middle and right depict the stop positions for super and sub-diffusion particles, respectively, coloured by a perceptually uniform sequential colormap based on their maximum displacement in the tiling space.

number of steps. It is a feature of the normal diffusive behavior. Fig. 3.8 shows how the difference between MSD of the particle and $4n$ varying over $\log_{10} n$ in LRWs. When $n \leq 4064.0$, the variation is not equal to 0 with larger fluctuation, which implies that blue, yellow, and pink particles undergo anomalous diffusion process. In other words,

$$\langle |\boldsymbol{r}(n)|^2 \rangle \propto n^{\gamma} \tag{3.2}$$

where $\gamma \neq 1$. In Fig. 3.10a, negative variation implies $\gamma < 1$ called sub-diffusion process, while positive value denotes $\gamma > 1$ named super-diffusion.

To understand the underlying mechanism of the anomalous-type diffusion process, initial and stop positions of particles in Fig. **??**, whose steps ranged from 4064 to 32586, are illustrated in Fig. 3.9. Suppose particles are trapped in the narrow space in-between the branches or initially start LRWs near the branching structure. In that case, their movements will be restricted because of the nearby absorbing boundary condition, causing the sub-diffusion phenomenon. As shown in the middle subplot of Fig. 3.9, the maximum displacement of sub-diffusion particles is less than 200. There also have exceptional circumstances that 6 particles, in-between the limbs, undergo super-diffusion since they can explore a large portion of space within a predefined range of steps, as shown in the right subfigure of Fig. 3.9. Generally, particles around the edges of the image will be more likely to pass through the periodic boundary, reappear in the adjacent cell, and continue LRWs with the same velocity until hitting the absorbing boundary, which results in large displacement and the super-diffusion process.

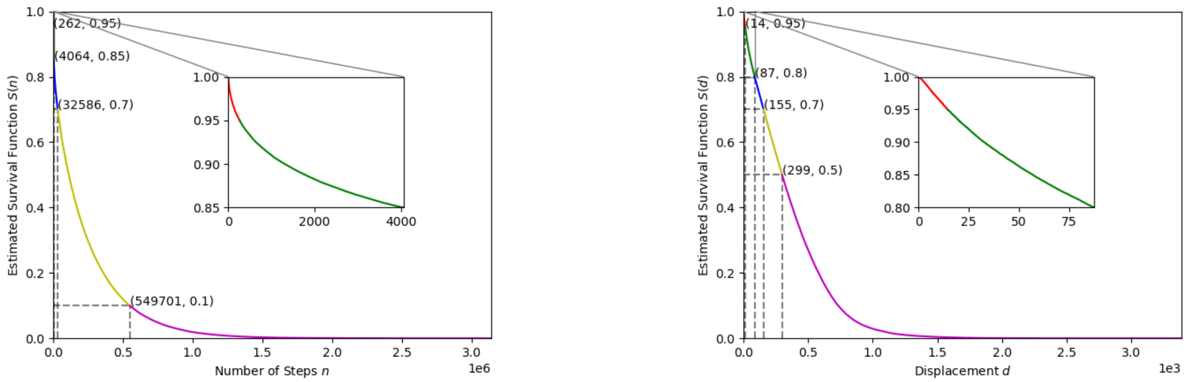

(a) (b)

Figure 3.10

		p			
		Log-rank	TW	GB	FH
G_1 L_3	G_1 L_4	0.4393	0.0285	0.0005	0.0005
	G_1 L_5	0.0	0.0	0.0	0.0
	G_1 L_6	0.0	0.0	0.0	0.0
G_1 L_4	G_1 L_5	0.0007	0.0	0.0	0.0
	G_1 L_6	0.0002	0.0	0.0	0.0
G_1 L_5	G_1 L_6	0.7223	0.0	0.0	0.0

Table 3.4: Two Sample Statistical Tests for $S(n)$ of G_1

3.3.2 Interpretation of Survival Curves

3.3.3 Comparison of Survival Curves

3.3.3.1 Distance Matrices

3.3.3.2 Multidimenisonal Scaling

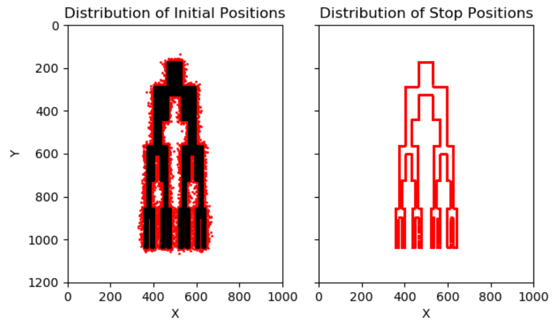

(a)

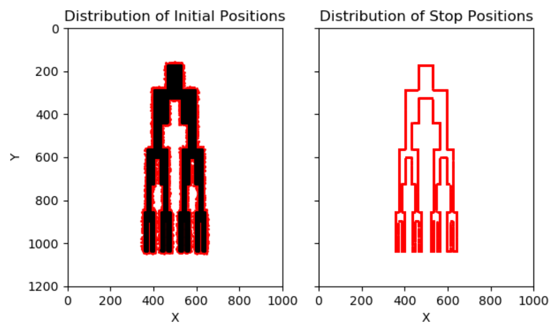

(b)

Figure 3.11

		p			
		Log-rank	TW	GB	FH
G_2 L_3	G_2 L_4	0.0	0.0	0.0	0.0
	G_2 L_5	0.0	0.0	0.0	0.0
	G_2 L_6	0.0	0.0	0.0	0.0
G_2 L_4	G_2 L_5	0.0016	0.0	0.0	0.0
	G_2 L_6	0.0004	0.0	0.0	0.0
G_2 L_5	G_2 L_6	0.7199	0.0	0.0	0.0

Table 3.5: Two Sample Statistical Tests for $S(n)$ of G_2

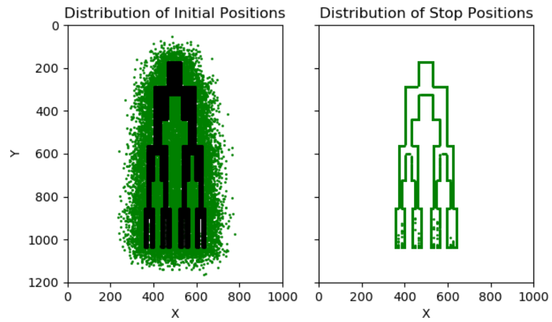

(a)

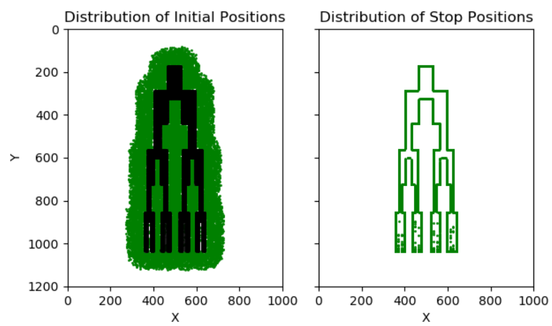

(b)

Figure 3.12

		p			
		Logrank	TW	GB	FH
$G_1\ L_3$	$G_1\ L_4$	0.0	0.0	0.0	0.0
	$G_1\ L_5$	0.0	0.0	0.0	0.0
	$G_1\ L_6$	0.0	0.0	0.0	0.0
$G_1\ L_4$	$G_1\ L_5$	0.0072	0.0	0.0	0.0
	$G_1\ L_6$	0.0003	0.0	0.0	0.0
$G_1\ L_5$	$G_1\ L_6$	0.2883	0.0	0.0	0.0

Table 3.6: Two Sample Statistical Tests for $S(d)$ of G_1

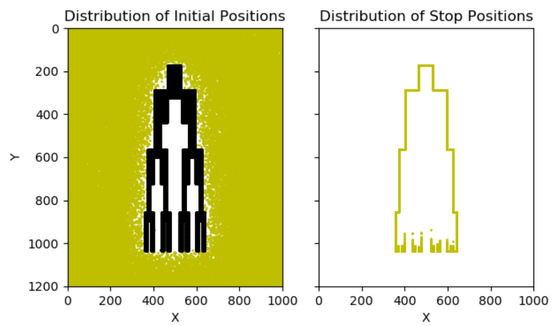

(a)

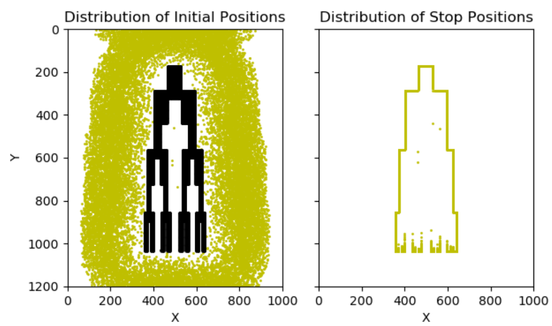

(b)

Figure 3.13

		p			
		Logrank	TW	GB	FH
G_2 L_3	G_2 L_4	0.0	0.0	0.0	0.0
	G_2 L_5	0.0	0.0	0.0	0.0
	G_2 L_6	0.0	0.0	0.0	0.0
G_2 L_4	G_2 L_5	0.0001	0.0	0.0	0.0
	G_2 L_6	0.0015	0.0	0.0	0.0
G_2 L_5	G_2 L_6	0.7019	0.0	0.0	0.0

Table 3.7: Two Sample Statistical Tests for $S(d)$ of G_2

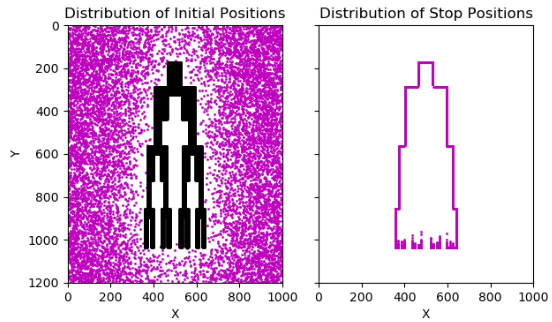

(a)

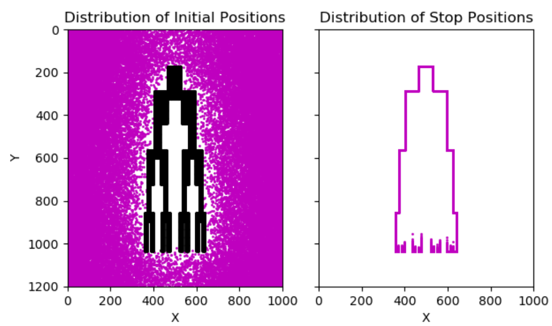

(b)

Figure 3.14

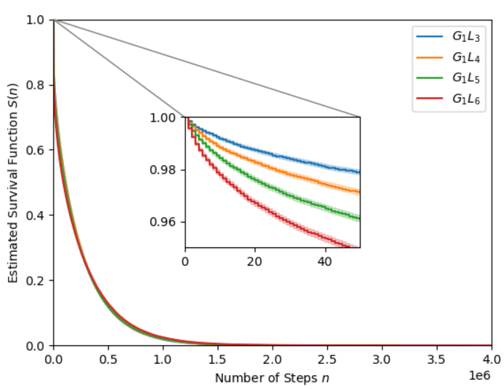

(a)

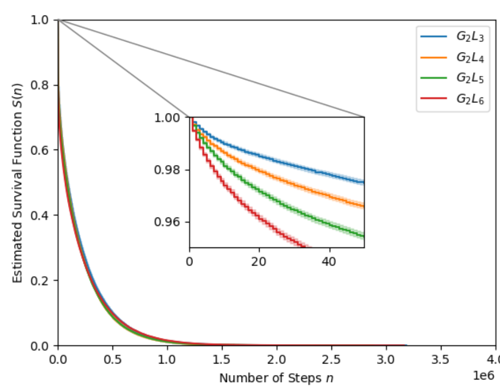

(b)

Figure 3.15: (a) and (b) are survival functions for branching structures in G_1 and G_2, respectively. n is the number of steps taken by the particle from the initial to the stop pixel in LRWs.

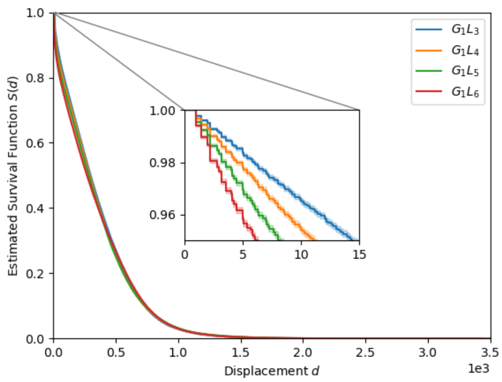

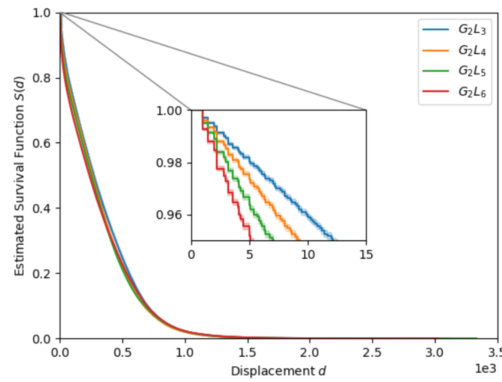

(a) **(b)**

Figure 3.16: (a) and (b) are the estimated survival functions associated with particles' displacement in LRWs in G_1 and G_2, respectively.

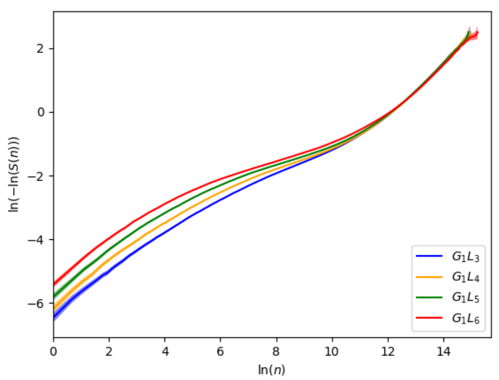

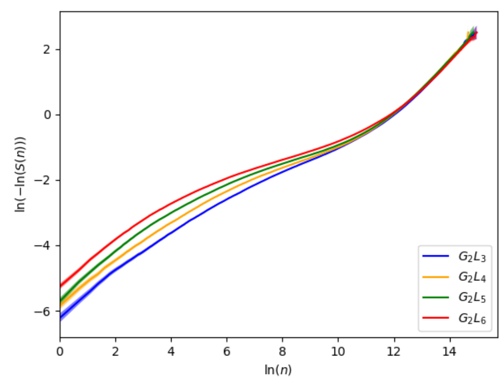

(a) **(b)**

Figure 3.17: (a) and (b) are commonly used graphical techniques to check the proportional hazards (PH) assumption of survival data by finding the parallelism. The survival distributions do not support the PH assumption since the hazard ratio in both G_1 and G_2 is not always constant.

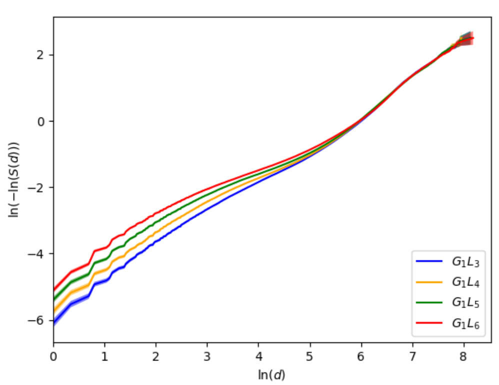

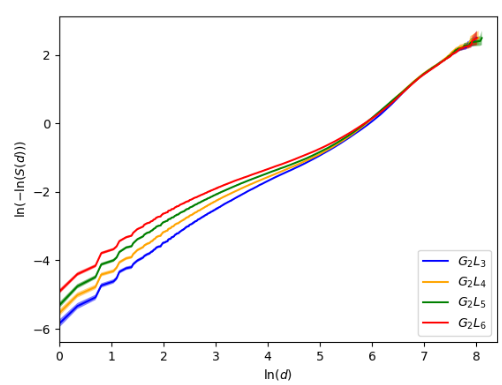

(a) **(b)**

Figure 3.18

3.4 Conclusion

- In a short time, the survival function of rectangle decays faster than the circle, which conforms to the analytical results.

- The differences of estimated survival functions between circle and rectangle are statistically significant, which coincides with the real shape dissimilarities.

- Within a same group, when t is small, the more branching the object is, the faster the survival function decays.

- Within a same group, the pairwise survival functions are statistically different.

- The corresponding target structures in G_1 and G_3 are invariant shapes under translation since their survival function are not statistically different. In other words, periodic boundary conditions of the image can eliminate the effect of the locations.

- LRWs can describe and classify the geometries, their spatial configurations, and the unoccupied area in the image.

LRWs in Real Root Images

Conclusion

Future Work

Appendix A

Numerical Methods for Solving Parabolic Partial Differential Equations

A.1 Introduction

- Parabolic PDEs: to characterize time-dependent phenomena
- The intrinsically similar features of the traditional computational techniques are mesh discretization in time and space.

A.2 Summary of Commonly Used Numerical Techniques

A.2.1 Finite Difference Method (FDM) [17]

A.2.2 Finite Element Method (FEM) [36]

A.2.3 Other Tranditional Computational Methods

A.3 Limitation in Practice

Appendix B

Method Validation in Annulus

B.1 Analytical Results

B.1.1 Shape Description

- Problem domain Ω: the region bounded by two concentric circles
- Radius of the larger circle: b
- Radius of the smaller circle: a

B.1.2 Solving Initial-Boundary Value Problem (IBVP)

B.1.2.1 Methods

- Dimensional Analysis: non-dimensional variables
  - $\mu = \frac{b}{a}$
  - $\tau = \frac{t}{a^2}$
  - $\hat{r} = \frac{r}{a}$
- Method of separation of variables

B.1.2.2 Mathematical Equations

- Diffusion equation

$$u_\tau = (u_{\hat{r}\hat{r}} + \frac{1}{\hat{r}}u_{\hat{r}} + \frac{1}{\hat{r}^2}u_{\theta\theta}) \tag{B.1}$$

- Uniform initial condition

$$u(\hat{r}, \theta, 0) = \frac{1}{|\Omega|} \tag{B.2}$$

- Homogenous Dirichlet B.C.

$$u(1, \theta, \tau) = 0 \tag{B.3}$$

- Homogenous Neumann B.C.

$$\hat{r}u'(\mu, \theta, \tau) = 0 \tag{B.4}$$

B.1.2.3 Heat Content Calculation

$$S(\tau) = \int_0^{2\pi} d\theta \int_1^{\mu} \hat{r} d\hat{r} u(\hat{r}, \theta, \tau) \tag{B.5}$$

B.2 Numerical Approximation

B.2.1 Eigenvalues $\lambda_{0,n}$

- Properties
  - $\lambda_{0,n} \in \mathbb{R}^+$, $(n \in \mathbb{N}_+)$
  - Monotonicity and Periodicity
- Estimation
  - $\lambda_{0,n} \in ((n-1)\pi, (n+1)\pi)$ [8]
  - Bisection method [34]

B.2.2 Approximation of $u(\hat{r}, \theta, \tau)$ and $S(\tau)$

- Direct summation
- Series acceleration methods

B.3 Comparison of Numerical and Analytical Results

B.3.1 Sample Size Evaluation

B.3.2 Comparison of $S(\tau)$ and $S(n)$

B.4 Conclusion

- The estimated survival function of LRWs is consistent with the analytical result.
- The number of particles in LRWs determined by DKW inequality is large enough to generate reproducible statistical results.

Appendix C

Artificial Images

C.1 Simple Shapes

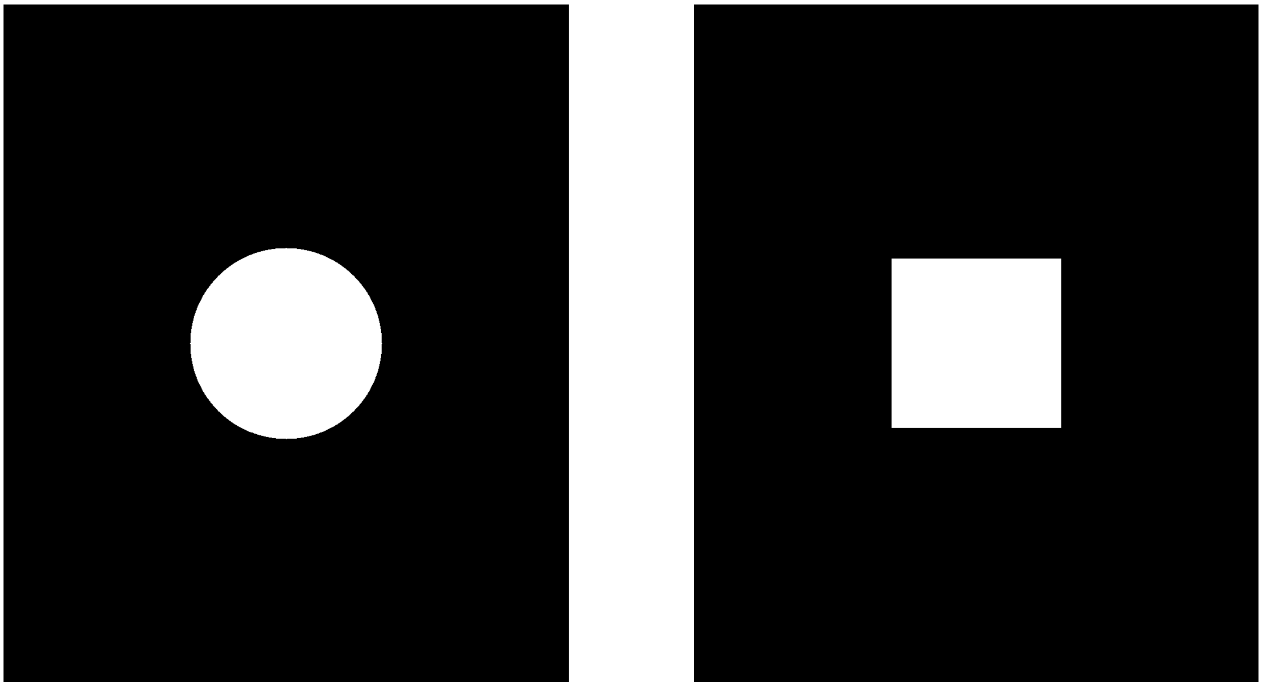

(a) Circle **(b)** Rectangle

Figure C.1: Each image size is 1200 by 1000 pixels with 90000 white pixels.

C.2 Complicated Branching Structures

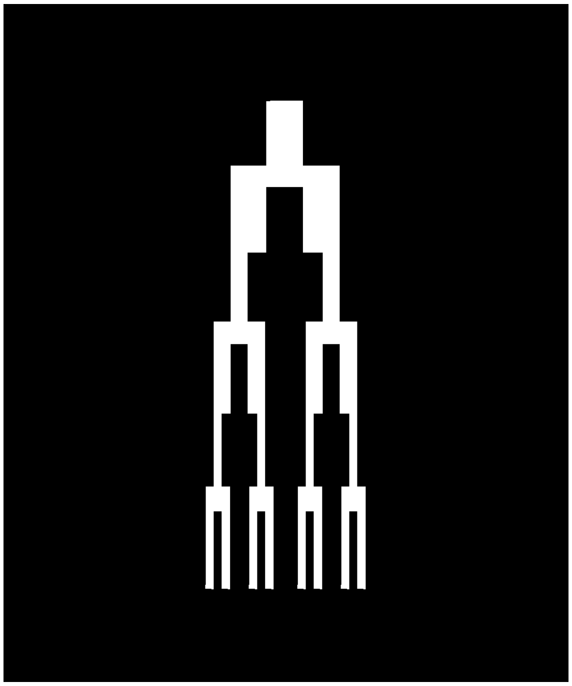

(a) G_1L_3

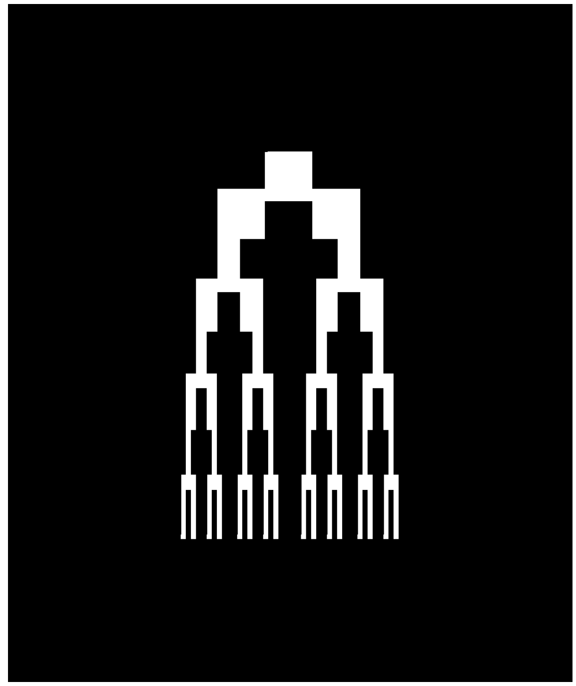

(b) G_1L_4

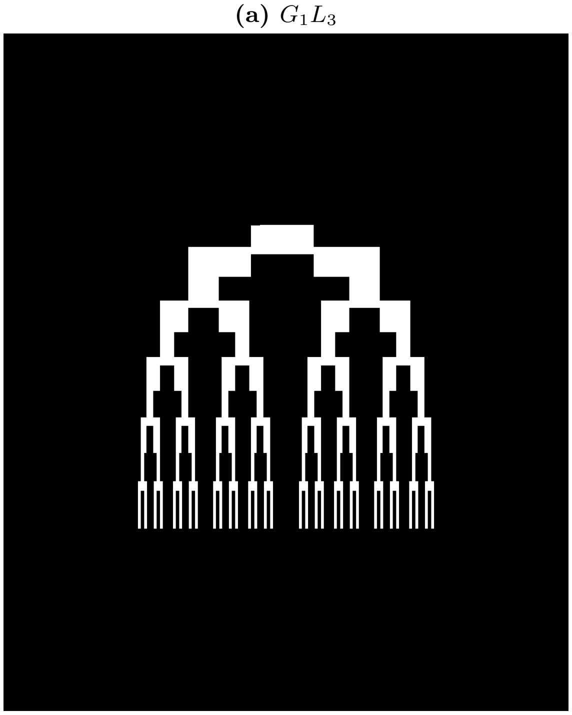

(c) G_1L_5

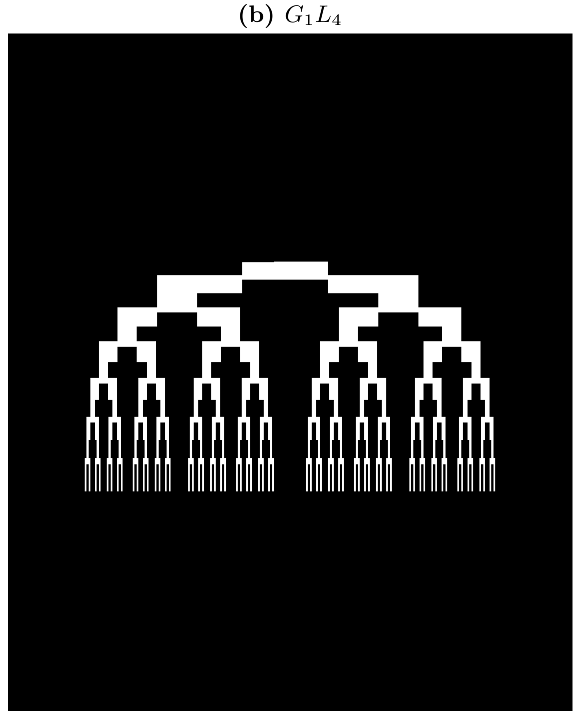

(d) G_1L_6

Figure C.2: In the group one, each image size is 1200 by 1000 pixels with 90000 white pixels.

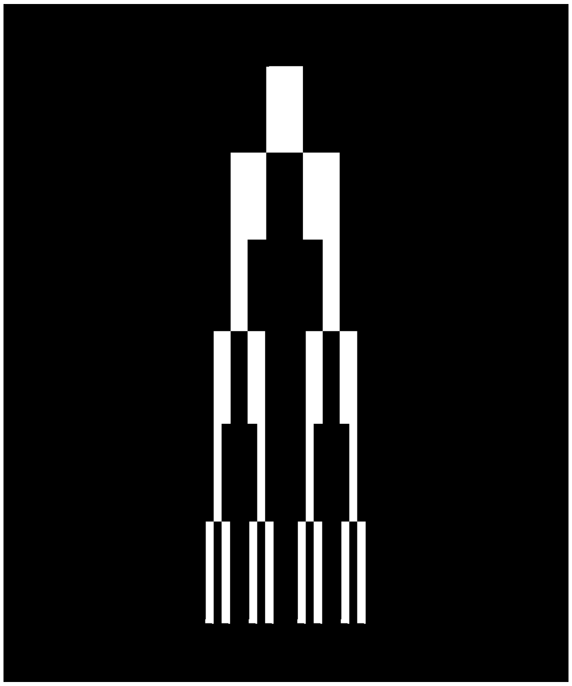

(a) G_2L_3

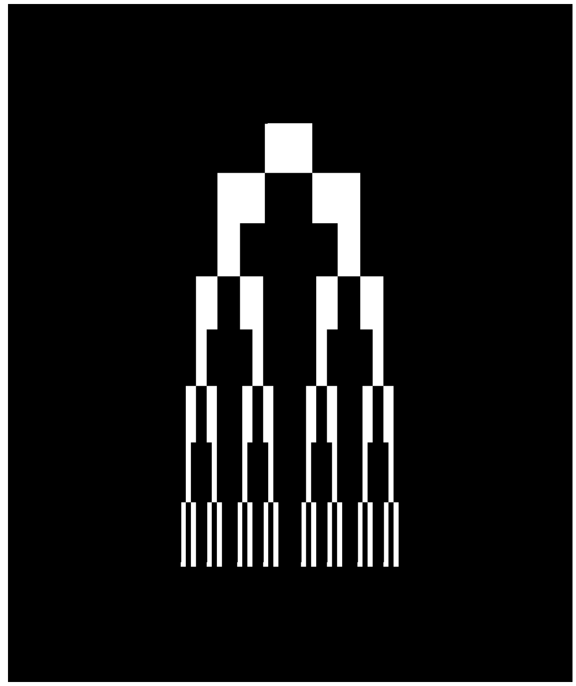

(b) G_2L_4

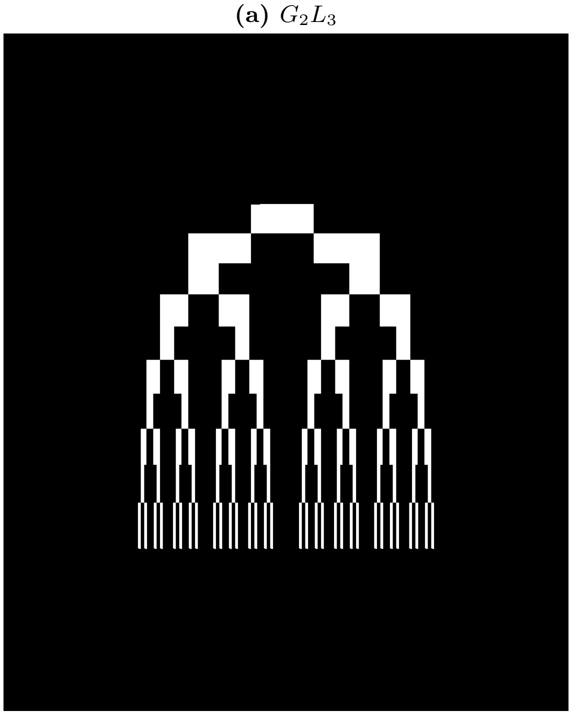

(c) G_2L_5

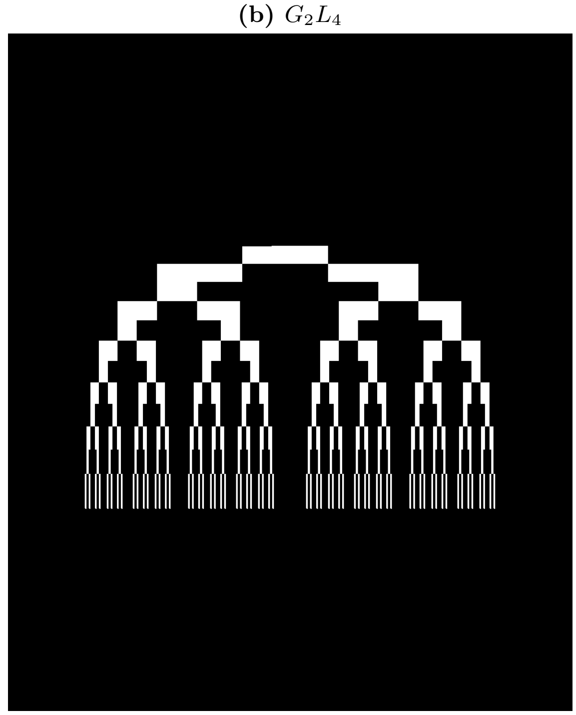

(d) G_2L_6

Figure C.3: In the group two, each image size is 1200 by 1000 pixels with 90000 white pixels.

References

[1] Odd Aalen, Ornulf Borgan, and Hakon Gjessing. *Survival and Event History Analysis: A Process Point of View*. Springer Science & Business Media, 2008.

[2] Girdhar Gopal Agarwal. Statistics for surgeons–understanding survival analysis. *Indian journal of surgical oncology*, 3(3):208–214, 2012.

[3] Mathilde Balduzzi, Brad M Binder, Alexander Bucksch, Cynthia Chang, Lilan Hong, Anjali S Iyer-Pascuzzi, Christophe Pradal, and Erin E Sparks. Reshaping plant biology: qualitative and quantitative descriptors for plant morphology. *Frontiers in Plant Science*, 8:117, 2017.

[4] Jean Baptiste Joseph Baron Fourier. *The analytical theory of heat*. The University Press, 1878.

[5] Ruvie Lou Maria Custodio Martinez. Diagnostics for choosing between log-rank and wilcoxon tests. 2007.

[6] Benjamin M Delory, Mao Li, Christopher N Topp, and Guillaume Lobet. archidart v3. 0: A new data analysis pipeline allowing the topological analysis of plant root systems. *F1000Research*, 7, 2018.

[7] S Desjardins and P Gilkey. Heat content asymptotics for operators of laplace type with neumann boundary conditions. *Mathematische Zeitschrift*, 215(1):251–268, 1994.

[8] *NIST Digital Library of Mathematical Functions*. http://dlmf.nist.gov/, Release 1.0.26 of 2020-03-15. F. W. J. Olver, A. B. Olde Daalhuis, D. W. Lozier, B. I. Schneider, R. F. Boisvert, C. W. Clark, B. R. Miller, B. V. Saunders, H. S. Cohl, and M. A. McClain, eds.

[9] Aryeh Dvoretzky, Jack Kiefer, and Jacob Wolfowitz. Asymptotic minimax character of the sample distribution function and of the classical multinomial estimator. *The Annals of Mathematical Statistics*, pages 642–669, 1956.

[10] İ Etikan, S Abubakar, and R Alkassim. The kaplan-meier estimate in survival analysis. *Biom Biostatistics Int J*, 5(2):00128, 2017.

[11] AH Fitter. The topology and geometry of plant root systems: influence of watering rate on root system topology in trifolium pratense. *Annals of Botany*, 58(1):91–101, 1986.

[12] AH Fitter and TR Stickland. Fractal characterization of root system architecture. *Functional Ecology*, pages 632–635, 1992.

[13] HPW Gottlieb. Hearing the shape of an annular drum. *The ANZIAM Journal*, 24(4):435–438, 1983.

[14] HPW Gottlieb. Eigenvalues of the laplacian with neumann boundary conditions. *The ANZIAM Journal*, 26(3):293–309, 1985.

[15] M Greenwood. The natural duration of cancer. london: His majesty's stationery office; 1926. *Reports on public health and medical subjects*, (33).

[16] Daniel Grieser and Svenja Maronna. Hearing the shape of a triangle. *Notices of the American Mathematical Society*, 60(11):1440–1447, 2013.

[17] Christian Grossmann, Hans-Görg Roos, and Martin Stynes. *Numerical treatment of partial differential equations*, volume 154. Springer, 2007.

[18] John M Hammersley. Monte carlo methods for solving multivariable problems. *Annals of the New York Academy of Sciences*, 86(3):844–874, 1960.

[19] David P Harrington and Thomas R Fleming. A class of rank test procedures for censored survival data. *Biometrika*, 69(3):553–566, 1982.

[20] David W Hosmer Jr, Stanley Lemeshow, and Susanne May. *Applied survival analysis: regression modeling of time-to-event data*, volume 618. John Wiley & Sons, 2011.

[21] Kurt Jacobs. *Stochastic processes for physicists: understanding noisy systems*. Cambridge University Press, 2010.

[22] Mark Kac. Can one hear the shape of a drum? *The American Mathematical Monthly*, 73(4P2):1–23, 1966.

[23] John D Kalbfleisch and Ross L Prentice. *The statistical analysis of failure time data*, volume 360. John Wiley & Sons, 2011.

[24] Edward L Kaplan and Paul Meier. Nonparametric estimation from incomplete observations. *Journal of the American statistical association*, 53(282):457–481, 1958.

[25] Pinar Gunel Karadeniz, Ilker Ercan, et al. Examining tests for comparing survival curves with right censored data. *Stat Transit*, 18(2):311–28, 2017.

[26] Mohamed A Khabou, Lotfi Hermi, and Mohamed Ben Hadj Rhouma. Shape recognition using eigenvalues of the dirichlet laplacian. *Pattern Recognition*, 40(1):141–153, 2007.

[27] E Leton and P Zuluaga. Equivalence between score and weighted tests for survival curves. *Communications in Statistics-Theory and Methods*, 30(4):591–608, 2001.

[28] Mao Li, Keith Duncan, Christopher N Topp, and Daniel H Chitwood. Persistent homology and the branching topologies of plants. *American Journal of Botany*, 104(3):349–353, 2017.

[29] S Sawyer. The greenwood and exponential greenwood confidence intervals in survival analysis. *Applied survival analysis: regression modeling of time to event data*, pages 1–14, 2003.

[30] BD Sleeman and EME Zayed. Trace formulae for the eigenvalues of the laplacian. *Zeitschrift für angewandte Mathematik und Physik*, 35(1):106–115, 1984.

[31] Jiro Tatsumi, Akira Yamauchi, and Yasuhiro Kono. Fractal analysis of plant root systems. *Annals of Botany*, 64(5):499–503, 1989.

[32] Zoltán Toroczkai. Topological classification of binary trees using the horton-strahler index. *Physical Review E*, 65(1):016130, 2001.

[33] Michiel Vandenberg and Peter B Gilkey. Heat content asymptotics of a riemannian manifold with boundary. *Journal of Functional Analysis*, 120(1):48–71, 1994.

[34] Pauli Virtanen, Ralf Gommers, Travis E. Oliphant, Matt Haberland, Tyler Reddy, David Cournapeau, Evgeni Burovski, Pearu Peterson, Warren Weckesser, Jonathan Bright, Stéfan J. van der Walt, Matthew Brett, Joshua Wilson, K. Jarrod Millman, Nikolay Mayorov, Andrew R. J. Nelson, Eric Jones, Robert Kern, Eric Larson, CJ Carey, İlhan Polat, Yu Feng, Eric W. Moore, Jake Vand erPlas, Denis Laxalde, Josef Perktold, Robert Cimrman, Ian Henriksen, E. A. Quintero, Charles R Harris, Anne M. Archibald, Antônio H. Ribeiro, Fabian Pedregosa, Paul van Mulbregt, and SciPy 1. 0 Contributors. SciPy 1.0: Fundamental Algorithms for Scientific Computing in Python. *Nature Methods*, 17:261–272, 2020.

[35] EME Zayed. Heat equation for an arbitrary doubly-connected region in $\mathbb{R}^2$ with mixed boundary conditions. *Zeitschrift für angewandte Mathematik und Physik*, 40(3):339–355, 1989.

[36] Miloš Zlámal. On the finite element method. *Numerische Mathematik*, 12(5):394–409, 1968.